Biosensors and Bioelectronics ■ (■■■■) ■■■–■■■

Contents lists available at ScienceDirect

Biosensors and Bioelectronics

journal homepage: www.elsevier.com/locate/bios

Multifunctional graphene micro-islands: Rapid, low-temperature plasma-enabled synthesis and facile integration for bioengineering and genosensing applications

Shafique Pineda [a,b,1], Fabricio Frizera Borghi [a,b,1], Dong Han Seo [a], Samuel Yick [a], Malcolm Lawn [c], Timothy van der Laan [a,b], Zhao Jun Han [a], Kostya Ken Ostrikov [a,b,d,*]

[a] CSIRO Manufacturing, P.O. Box 218, 36 Bradfield Road, Lindfield, NSW 2070, Australia
[b] School of Physics, The University of Sydney, Sydney, NSW 2006, Australia
[c] National Measurement Institute (NMI), Nanometrology, 36 Bradfield Road, Lindfield, NSW 2070, Australia
[d] Institute for Future Environments and Institute for Health and Biomedical Innovation, School of Chemistry, Physics, and Mechanical Engineering, Queensland University of Technology, Brisbane QLD 4000, Australia

ARTICLE INFO

Article history:
Received 23 December 2015
Received in revised form
20 April 2016
Accepted 21 April 2016

Keywords:
Low-temperature plasma
Plasma nanoscience
Graphene
Biosensor
Biocompatibility
Biomaterials

ABSTRACT

Here, we present a rapid, low-temperature (200 °C) plasma-enabled synthesis of graphene micro-islands (GMs). Morphological analyses of GMs by scanning electron microscopy (SEM) and atomic force microscopy (AFM) feature a uniform and open-networked array of aggregated graphene sheets. Structural and surface chemical characterizations by Raman spectroscopy and X-ray photoelectron spectroscopy (XPS) support the presence of thin graphitic edges and reactive oxygen functional groups. We demonstrate that these inherent properties of GMs enable its multifunctional capabilities as a bioactive interface. GMs exhibit a biocompatibility of 80% cell viability with primary fibroblast lung cells after 5 days. Further, GMs were assembled into an impedimetric genosensor, and its performance was characterized by electrochemical impedance spectroscopy (EIS). A dynamic sensing range of 1 pM to 1 nM is reported, and a limit of quantification (LOQ) of 2.03×10^{-13} M is deduced, with selectivity to single-RNA-base mismatched sequences. The versatile nature of GMs may be explored to enable multi-faceted bioactive platforms for next-generation personalized healthcare technologies.

1. Introduction

Graphene, an atomically-thin film of crystalline carbon, has attracted significant interest for biomedical technologies owing to its exceptional physicochemical properties, determined by its unique two-dimensional structure and morphology (Novoselov et al., 2012). However, green and resource-efficient production of graphene and its facile integration into biomedical devices are essential for such technologies to be feasible, which remains a challenge (Zurutuza and Marinelli, 2014).

Recent investigations have demonstrated significant progress in addressing several of these concerns to facilitate the utilization of graphene technologies in biomedical applications. This includes reducing the production cost of graphene films grown by thermal chemical vapor deposition (CVD), by using lower growth temperatures and other carbon precursors (Guermoune et al., 2011; Sun et al., 2010). However, these techniques still involve long processing times and notably high temperatures (~850 °C). Moreover, while graphene dispersions prepared by chemical exfoliation are cheaper alternatives to CVD grown graphene films, their synthesis requires multi-staged complex processing, often in harsh chemical environments (Hernandez et al., 2008). Also, such graphene dispersions tend to agglomerate, and utilization of graphene as a functional surface requires additional chemical binders (Li et al., 2008). While these graphene dispersions have shown good biocompatibility, their uses are limited by a poor electrical conductivity and a resource-consuming integration, which undermines its performance and multifunctionality for applications in bioelectronics.

In addition, there have been efforts to improve the integration of graphene into electronics, by utilizing either dry transfer techniques or improved transfer techniques based on reactive chemical etching (Gao et al., 2012; Suk et al., 2011). However, these approaches are multi-staged and involve complex handling of graphene, and often introduce cytotoxic impurities on the surface of graphene. It is thus important to develop a simple, fast, environmentally-benign, low-temperature graphene production and

* Corresponding author at: CSIRO Manufacturing, P.O. Box 218, 36 Bradfield Road, Lindfield, NSW 2070, Australia.
E-mail address: kostya.ostrikov@csiro.au (K.K. Ostrikov).
[1] These authors contributed equally to this work.

http://dx.doi.org/10.1016/j.bios.2016.04.072
0956-5663/

integration for bioelectronics.

Plasma has been shown to grow multilayer graphene flakes, containing single layer graphene domains of sub-micrometre to just-above-micrometre size (van der Laan et al., 2015). However, such graphene flakes are sparsely grown, and thus, remain unfavorable for use as bioactive coatings and biosensing interfaces, whereby a larger quantity, surface coverage, and better transferability of graphene are required. Herein, graphene micro-islands (GMs) are synthesized by a low-temperature plasma, that is resource-efficient and eco-friendly. We demonstrate the multifunctionality of GMs as a bioactive interfacial material for biocompatible coatings and electrochemical genosensing.

2. Materials and methods

2.1. Plasma-enabled growth of GMs and water-mediated transfer

The deposition of GMs was carried out in a RF inductively coupled plasma CVD system. A copper foil (99.5%, Alfa Aesar) of dimensions 4 cm × 4 cm was used as growth substrate for the GMs. Firstly, a gas mixture of 10 sccm Ar and 90 sccm H_2 was fed into the chamber, and then the plasma was generated at a pressure of 2.0 Pa and RF power of 750 W, respectively. The copper foil was treated with Ar/H_2 plasma for 3 min. Next, 2 sccm of CH_4 was fed into the chamber. Although no external substrate heating was used, during a subsequent 8 min deposition process, the substrate temperature reached ~200 °C due to the plasma-heating effects. Next, the GMs were decoupled from the copper foil by immersion in de-ionized water. GMs floated as a film on the water surface, and were transferred onto a glass microslide for subsequent characterizations.

2.2. Microscopy and microanalysis

Field-emission scanning electron microscopic (FE-SEM) images were obtained by Zeiss Auriga microscope operated at 5 keV electron beam energy with an InLens secondary electron detector. Atomic force microscopy (AFM) images were acquired with an Asylum Research MFP-3D AFM operating in intermittent contact ("tapping") mode with a 5 N/m spring constant cantilever. Image analysis was performed using the Scanning Probe Image Processor (SPIP™) software produced by Image Metrology A/S. Raman spectroscopy was performed using a Renishaw inVia spectrometer with a laser excitation at 514 nm (Ar laser) and a probing spot size of ~1 μm^2. X-ray photoelectron spectroscopy (XPS) spectra were recorded by Specs SAGE 150 spectroscope with the Mg Kα excitation at 1253.6 eV. Both survey and narrow scans of C 1s were conducted.

2.3. Biosensing measurements

The size of each sensing substrate was 2 cm × 1 cm. The biosensing electrode consisted of GMs on aluminium foil. Subsequently, the GMs were treated with 0.05 M *N*-(3-Dimethylaminopropyl)-*N*′-ethylcarbodiimide hydrochloride (EDC) and 0.03 M N-hydroxysulfosuccinimide (NHS) in phosphate buffered saline (PBS, pH =7, Sigma Aldrich) for 15 min. This enabled the formation of active ester intermediates via carbodiimide chemistry. Next, the surface of graphene was washed several times with PBS and DI water to remove excess EDC/NHS. Then, NH_2-conjugated miRNAs (probe sequence: 5′-NH_2-AUUUCACGACUGUCACGUCUA-3′, Sigma Aldrich) were diluted in PBS to 0.2 μM, and 50 μL was pipetted onto the EDC/NHS-treated surface. This was left to incubate overnight in a wet environment at room temperature. Next, the sensing surface was washed with 0.05% sodium dodecyl sufonate (SDS) (Sigma Aldrich) in 0.04 M hydroxylamine solution (Sigma Aldrich) to deactivate the remaining carboxyl functional groups and to remove non-specifically bound probe miRNAs. Then, 0.01 M Polyethylene glycol (PEG) (Sigma Aldrich) was loaded on the sensing surface to block the exposed areas of graphene to reduce further non-specific binding. The (biomarker) miRNA sequence (target sequence: 5′-UAAAGUGCUGACAGUGCAGAU-3′, Sigma Aldrich) was dissolve in human serum (Human Plasma AB, Sigma Aldrich) to obtain dynamic concentrations of 1 pM–1 nM, which were pipetted onto the sensing surface. This was left to incubate at 45 °C for 20 min to induce hybridization between the complementary probe and target sequences. Finally, a washing step with PBS/DI water was employed to remove remaining non-specifically bound target miRNAs. To demonstrate sensing specificity, a similar protocol was adopted by replacing the target sequence with a single-RNA-base mismatched sequence (non-complementary sequence: 5′-UAGAGUGCUGACAGUGCAGAU-3′, Sigma Aldrich). This fully assembled device was then utilized in a three-electrode electrochemical cell for biosensing measurements.

2.4. Cytotoxicity testing

The cytotoxicity of plasma-grown GMs was evaluated using CellTiter 96 Aqueous Non-Radioactive Cell proliferation (MTS) Assay (Promega, C#G5421) following the protocol provided by the manufacturer. Primary fibroblasts lung cells (MRC5 cell line) were cultured in 96-well plates at 2 × 10^4 cells/well on control (Tissue Culture Polystyrene – TCPS), glass and glass covered with GMs for 1–5 days. Optical microscopy images were taken after 24 h and 120 h of culture, on the 1 day and 5 days samples, respectively.

3. Results and discussion

3.1. Fabrication and characterization of graphene micro-islands

The procedure for preparing GMs is illustrated in Fig. 1A. A low-temperature plasma process enables the growth of GMs on a copper foil. This approach is typically more resource-efficient compared to chemical vapor deposition (CVD) and represents an environmentally-benign alternative to conventional wet-chemical methods, which involve high temperatures and hazardous chemicals, respectively (Biswal et al., 2013).

During the early growth process (~2 min), the methane is rapidly dissociated into carbon building units by the plasma. Subsequently, these carbon species reorganize into hexagonal carbon-rings forming graphene nanosheets. Such plasma-unique effects are mainly attributed to the strong plasma-matter interactions in the plasma sheath (Ostrikov et al., 2013; Yick et al., 2013). In particular, hydrogen may enhance the surface flux of these building units through the recombination-mediated energy dissipation on the surface and facilitate the nucleation and growth of graphene nanosheets (Seo et al., 2013). Fig. 1A outlines the process for GM synthesis. Initially, graphene nanosheets grow vertically from the substrate due to the electric field in the plasma sheath (Supplementary Fig. S1). Upon water-mediated transfer, the vertically-standing graphene nanosheets collapse to lay horizontally on the transferred substrate, in a two-dimensional open and arrayed network of GMs. Additionally, the controlled growth of GMs and its reproducibility are studied in Supplementary Fig. S2.

The microstructure and morphology of GMs are examined in Fig. 1B–D, with scanning electron microscopy (SEM) and atomic force microscopy (AFM) topography imaging. The GMs are outlined in the high-magnification SEM image (Fig. 1B). GMs are deduced to be composed of graphene domains (each 200–500 nm in dimension), aggregated in an open network of micron-sized

Please cite this article as: Pineda, S., et al., Biosensors and Bioelectronics (2016), http://dx.doi.org/10.1016/j.bios.2016.04.072

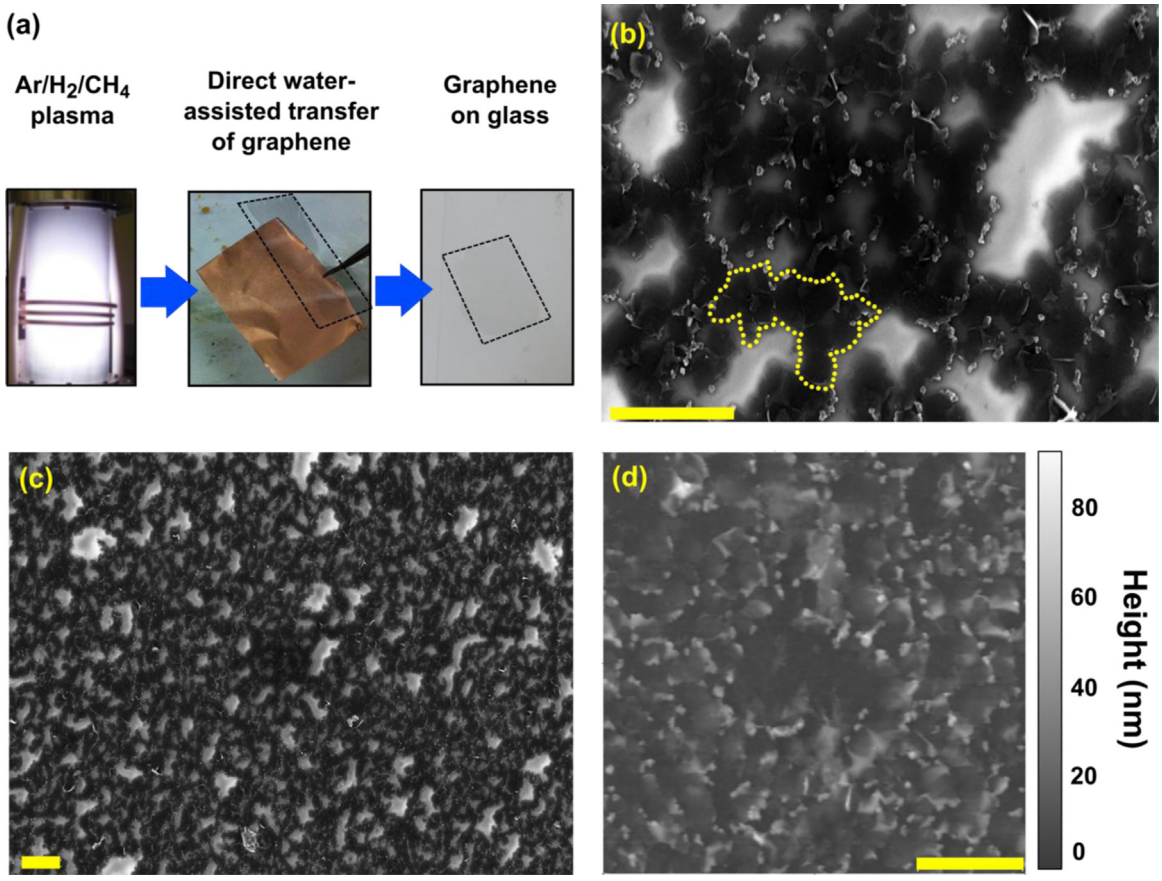

Fig. 1. (A) Low-temperature plasma process for the synthesis of graphene micro-islands (GMs). High-magnification SEM (B) features GMs outlined in yellow. Low-magnification SEM (C) shows the uniform large-area coverage of GMs. (D) AFM topography imaging of GMs. Scale bars correspond to 1 μm. (For interpretation of the references to color in this figure legend, the reader is referred to the web version of this article.)

islands. These GMs are observed to provide a uniform surface coating (Fig. 1C). AFM topography imaging of GMs (Fig. 1D) feature graphene sheets (< 20 nm) inter-connected in an arrayed morphology, and the presence of carbon clusters (~60 nm) along the edges of the graphene islands. Notably, these carbon clusters may be attributed to nucleation regions for the growth of graphene nanosheets in the plasma process. The morphology of individual GMs is further investigated with a close-up 3D AFM topographic map (Supplementary Fig. S3). Together, SEM and AFM characterizations confirm the inter-connected and open morphology of GMs.

The structural and chemical compositions of GMs are characterized by Raman and X-ray photoelectron spectroscopy (XPS). Three distinct peaks are present (Fig. 2A), namely, the characteristic disorder peak (D-band) at 1350 cm^{-1}, the graphitic peak (G-band) at 1580 cm^{-1}, and the second-order 2D-band at 2690 cm^{-1}. The G-band arises from the in-plane vibrational E_{2g} mode of the sp^2-hybridized carbon, the D-band is attributed to the finite crystallite size effect and various defects induced in the sp^2 carbon materials, and the 2D-band is a second-order Raman spectral feature due to the three-dimensional inter-planar stacking of hexagonal carbon networks (Cuesta et al., 1998; Lespade et al., 1982; Niyogi et al., 2011; Wang et al., 1990). Further, Raman spectral mapping was conducted to examine the uniformity of GMs (Fig. 2B–C). The characteristic peaks feature intensity ratios of I_{2D}/I_G~(1.60–2.10) and I_D/I_G~(1.10–1.30), which indicate the presence of homogeneously thin and reactive sheets of graphene (Niyogi et al., 2011; Ruan et al., 2011) with enhanced electrochemical activity (Seo et al., 2015).

The chemical composition of GMs was analyzed by X-ray photoelectron spectroscopy (XPS). The survey scan (Fig. 2D) shows dominant peaks at binding energies of 284.5 eV (C 1s) and 532.7 eV (O 1s). The C 1s spectrum in Fig. 2E can be de-convoluted into six components, corresponding to sp^2 (284.5 eV), sp^3 (285.4 eV), C–O–C bonds (286.2 eV), C=O bonds (287.4 eV), O–C=O bonds (289.4 eV) and π–π^* satellite orbitals (291.5 eV) (Hsiao et al., 2010). Notably, such sp^3 clusters contribute to an increase in I_D/I_G. Further, an O 1s spectrum centered at 532.7 eV supports the presence of such oxygen-attached carbon species (Supplementary Fig. S3). GMs feature a sp^2 and sp^3 compositions of 68% and 12.5%, respectively, which indicates graphitic quality consistent with Raman characterizations. These oxygen moieties may have been introduced through its open edges, either following the immediate exposure of GMs to air, or through the water-mediated transfer process. Thus, Raman and XPS characterizations affirm that plasma-derived GMs possess reactive graphitic edges and oxygen functionalities.

Together, the morphological and chemical features of GMs may not only facilitate the access and surface immobilization of biological analytes, but also, may enable GMs to be readily available for integration as an interfacial material for bioengineering or electrochemical sensing applications.

3.2. Biocompatibility of graphene micro-islands

Plasma-grown GMs present surface defects, oxygen functionalities, and a large surface area. Such morphological and chemical features of GMs may increase its surface energy and polarity, which may favour the proliferation of cells (Borghi et al., 2013; Wang et al., 2006). Furthermore, the plasma-unique growth and

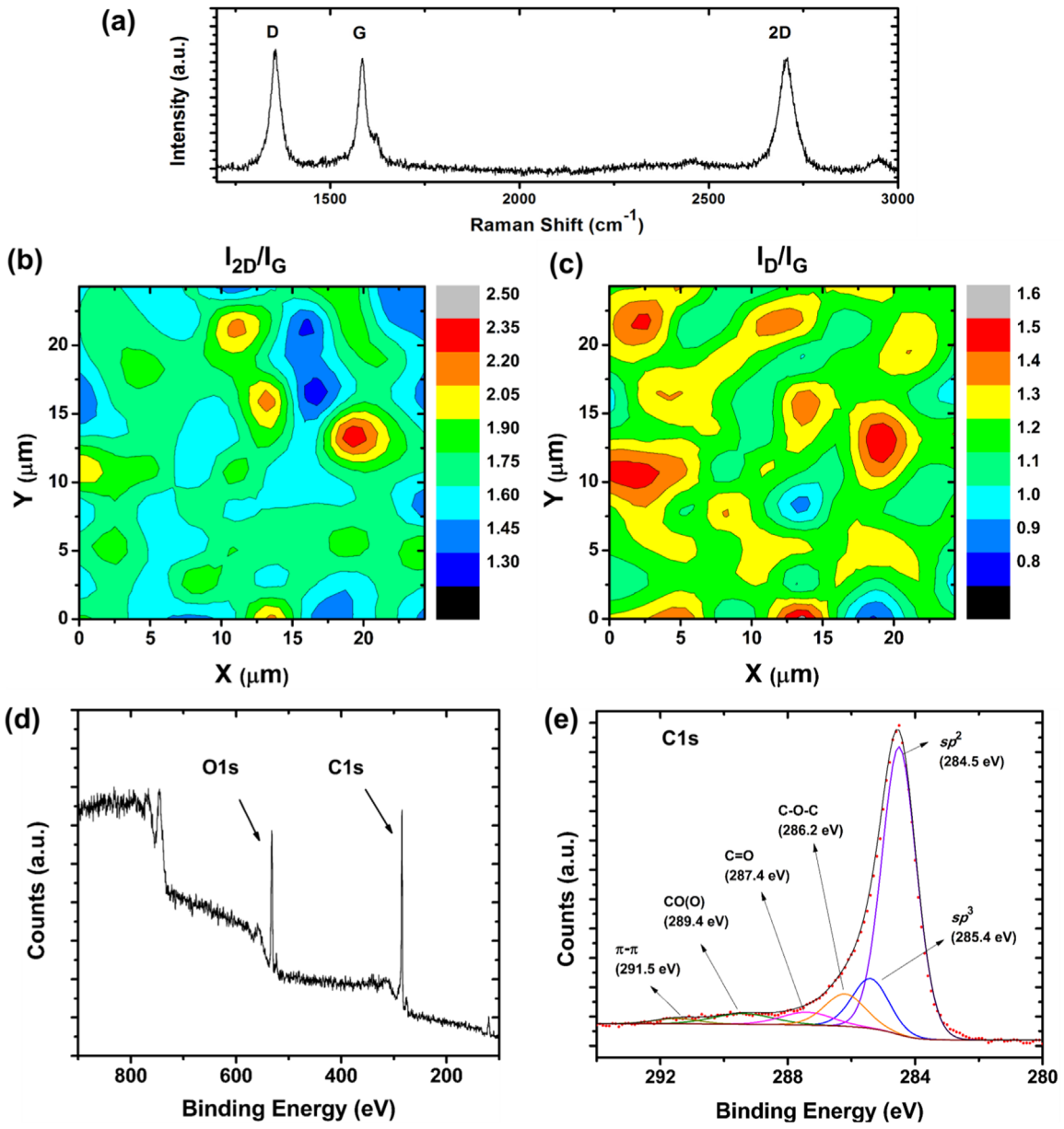

Fig. 2. Structural and surface chemical characterizations of graphene micro-islands (GMs). (A) A typical single-point Raman spectrum of GMs. (B) and (C) Raman spectral mapping of characteristic peak ratios ($I_{2D/G}$ and $I_{D/G}$) for GMs over a 25 μm × 25 μm area. (D) XPS survey scan and respective (E) C 1s narrow spectrum of GMs.

water-mediated transfer process allows GMs to be transferred to arbitrary substrates with minimal contamination.

The toxicity assay was used to study cell viability on the first and fifth days, where the cell counts were normalized by using the data for the control samples after day 1 (Fig. 3A). The cell viability over the five days showed that all samples induce and sustain cell growth (higher than 80%) with a small decrease of the number of living cells observed for all samples.

This is supported by the micrographs that show the altered morphology and cell counts when compared to control samples (Fig. 3B). The morphology of cells was used to determine the progression of cell proliferation in the first 24 (first row) and 120 h (second row). From the micrographs, the cells were determined to proliferate equally on the glass surface and the GMs. After 5 days of cell culture, fewer cells were observed to be attached on the surface of GMs as compared to the first day. The cells on the control substrate were more spread out, presumably due to the different stiffness and optimized treatments applied on these surfaces for cell growth. These biocompatibility results are comparable to *in vitro* studies of graphene-based materials on the viability of mammalian cell lines. For instance, it was shown that the survival rate of human cervical cancer cells on graphene oxide was 75–85% after 48 h (Hong et al., 2012), and the survival rate of HeLa cancer cells on graphene oxide was 80–90% after 24 h (Peng et al., 2010; Yang et al., 2012). These results suggest that GMs represent a good interfacial material for the adhesion and proliferation of primary fibroblast lung cells. In other words, plasma-grown GMs are biocompatible and may be suitable for bioengineering applications.

3.3. Graphene micro-islands for biosensing

Electrochemical sensing methods for minute amounts of nucleic acid samples offer attractive opportunities for a plethora of preventative health technologies, which require portable, cost-effective, and low-power readout devices (Turner, 2013). Diseases such as cancers are becoming more prevalent with the growing population. Importantly, cancers may be best managed with early

Please cite this article as: Pineda, S., et al., Biosensors and Bioelectronics (2016), http://dx.doi.org/10.1016/j.bios.2016.04.072

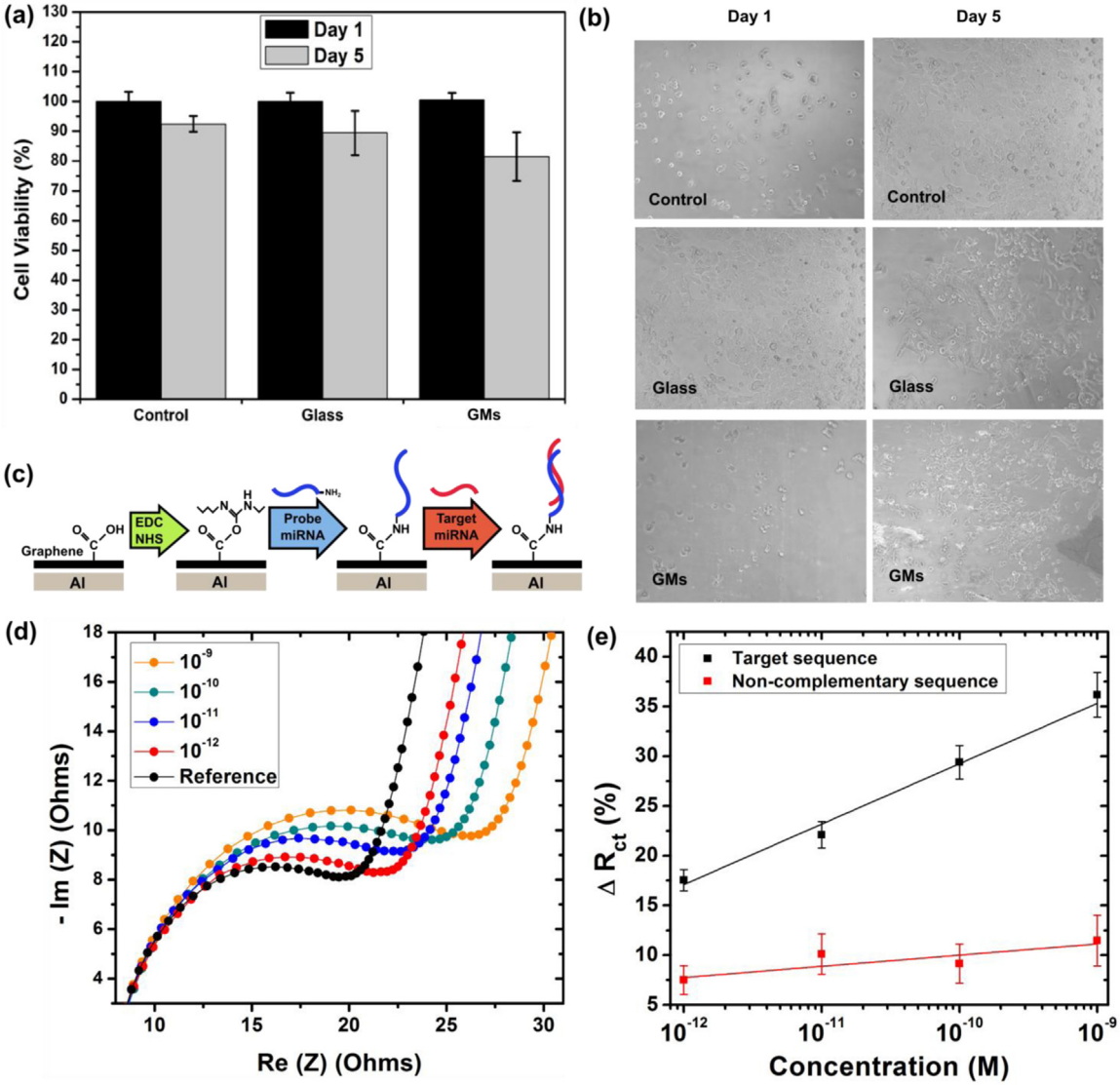

Fig. 3. Biocompatibility and biosensing performances of graphene micro-islands (GMs). Cell viability of graphene micro-islands (GMs) evaluated (A) over 5 days of incubation, with (B) respective optical images of cell cultures. (C) Schematic for the assembly of an electrochemical biosensor based on graphene micro-islands (GMs). (D) and (E) Electrochemical impedance spectroscopy (EIS) response for GM-based biosensor with respect to the target miRNA and a single-RNA-base mismatched sequence. ΔR_{ct} is defined by $(R_{ct}-R_0)/R_0$, where R_0 is the charge-transfer resistance of the reference sample. Corresponding data are summarized in Table 1.

intervention therapies followed by early-stage diagnosis. Recently, post-transcriptional epigenetic regulations of gene expressions have been found to provide highly-valuable serum-based nucleic acid biomarkers which may be utilized to enable early diagnostic strategies for breast cancer (Gong et al., 2015, 2014). Consequently, the favourable morphology and chemical features of GMs motivates its consideration as a biosensing electrode.

Assembly of the electrochemical GM-based biosensor is illustrated in Fig. 3C. Plasma-grown GMs feature active carboxyl functionalities on its surface. Through carbodiimide chemistry, this facilitates the covalent immobilization of probe miRNAs, and enables the specific detection of the complementary miRNA sequence.

Performance of the GM sensor was quantified by electrochemical impedance spectroscopy (EIS) technique. The charge transfer resistance (R_{ct}) was measured to characterize the response of GMs to the surface immobilization of miRNAs. Fig. 3D and E demonstrates an increase in ΔR_{ct} as the concentration of target miRNAs was increased. We define ΔR_{ct} by $(R_{ct}-R_0)/R_0$, where R_0 is the charge-transfer resistance of the reference sample. This increase in ΔR_{ct} may be attributed to a retarded charge transport towards the GM surface, either through spatial blocking or electrical repulsion. In particular, the hybridization between complementary genomic sequences induces a build-up of negative surface charge, and the repulsion of negatively charged ferricyanide ions, which leads to a rise in R_{ct} (Suni, 2008). Further, this GM-based sensor demonstrates selectivity against miRNA sequences that are mismatched by a single RNA base. A slight increase in R_{ct} was observed at elevated concentrations of non-complementary miRNA. This may be attributed to an increase in non-specifically adsorbed miRNAs on the surface of GMs. Correspondingly, these biosensing data are summarized in Table 1.

The impedance response of GMs in the presence of target miRNAs was analyzed by linear regression (Fig. 3E). A relation of $\Delta R_{ct}=89.99+6.07log_{10}$ (*Concentration* [M]), $R^2=0.98$, was deduced (black curve). The limit of quantification (LOQ) was calculated by $10S_y/b$, with S_y as the standard deviation of the y-intercept ($S_y=7.83$), and b as the slope of the linear fit ($b=6.07$) (Armbruster and Pry, 2008; Shrivastava and Gupta, 2011). GMs report a dynamic sensing range that spans 1 pM to 1 nM, and a LOQ of 2.03×10^{-13} M. These performances of GMs are comparable or better than graphene-based electrochemical sensors reported in

Please cite this article as: Pineda, S., et al., Biosensors and Bioelectronics (2016), http://dx.doi.org/10.1016/j.bios.2016.04.072

Table 1
Table of data for impedimetric response of graphene micro-islands (GMs), as presented in Fig. 3D and E.

Concentration (M)	Average R_{ct} (Ohms)	Error R_{ct} (Ohms)	ΔR_{ct} (%)	Error ΔR_{ct} (%)
0 (Reference)	15.65 (R_0)	0.35	–	–
Target sequence				
10^{-12}	18.39	0.31	17.55	1.08
10^{-11}	19.10	0.30	22.09	1.33
10^{-10}	20.25	0.26	29.39	1.67
10^{-9}	21.31	0.41	36.17	2.29
Non-complementary sequence				
10^{-12}	16.82	2.50	7.49	1.45
10^{-11}	17.23	2.72	10.12	2.04
10^{-10}	17.08	2.89	9.16	1.95
10^{-9}	17.44	3.12	11.46	2.55

recent literature. Notably, chemically-derived reduced graphene oxide (RGO) has been widely utilized in the assembly of such electrochemical sensors. However, GO dispersions agglomerate uncontrollably when reduced, leading to poor graphene morphology, diminished graphene properties, and a reduction of active surface area for sensing. Additionally, the integration of GO dispersions into an electrode typically involves non-conductive surfactants or chemical binders. This significantly increases the impedance of the sensor, and leads to a compromise in sensitivity. Also, the preparation of RGO powders involves a long, multi-staged process and harsh chemicals. For instance, GO decorated with perylene tetracarboxylic acid diimide (PDI) have been utilized to enable a detection limit of 5.5×10^{-13} M single-stranded (ss) DNA (Hu et al., 2012). Similarly, RGO have been functionalized with tryptamine to achieve a limit of detection of ssDNA 5.2×10^{-13} M ssDNA (Zhang et al., 2014). Also, graphite fibers have been activated to form GO interfaces capable of detecting ssDNA down to concentrations of 5.6×10^{-12} M (Zhang et al., 2015). Thus, the unique morphological and surface chemical properties of GMs enable its facile integration as an impedance sensor, capable of sensitive and selective detection of miRNA. These results may be promising for future developments of early diagnostic strategies for cancer, which require the quantification of multiple biomarkers in complex biological environments. Furthermore, electrochemical genosensors based on GMs may be tailored to detect the onset and monitor the progression of other debilitating diseases.

4. Conclusion

In summary, we have presented a plasma-enabled low-temperature synthesis and water-mediated transfer of GMs. Morphological analyses by SEM and AFM reveal that GMs feature a uniform and open-networked array of aggregated graphene sheets. Structural and surface chemical characterizations by Raman spectroscopy and XPS support the presence of thin graphitic edges and reactive oxygen functional groups. We have demonstrated that these inherent properties of GMs enable its multifunctional capabilities for biocompatible coatings and electrochemical sensing. GMs exhibited a biocompatibility of 80% cell viability with primary fibroblast lung cells after 5 days. Also, GMs were assembled to realize an impedimetric biosensor for miRNAs. A dynamic sensing range of 1 pM to 1 nM was reported, and a limit of quantification of 2.03×10^{-13} M was deduced, with selectivity to single-RNA-base mismatched sequences. We envision that GMs are promising for future developments in wearable organic electronics. In principle, the active surface of GMs may enable a multitude of functionalities by hosting various heterostructures and nanocomposites. This may facilitate diverse capabilities in sensing, bioengineering, and anti-microbial coatings. For instance, GMs may be coupled to flexible polymer substrates or textiles to enable multi-faceted platforms for next-generation biomedical devices. We propose these subsequent investigations for the ongoing development of plasma-enabled medical technologies.

Acknowledgements

This work is supported by the Australian Research Council (ARC) and CSIRO's Office of the Chief Executive (OCE) Science Leader Program. S.P. acknowledges the support from the Australian Postgraduate Award (APA) and CSIRO's OCE top-up scholarship. F.F.B acknowledges the scholarship support from the National Council for Science and Technology Development (CNPq – Brasil). T.V.D.L. acknowledges the support from the APA. D.H.S and S.Y. acknowledge the CSIRO's OCE Postdoctoral Fellowship Program. Z.J.H. and K.O. acknowledge the support from the DECRA and Future Fellowships from the ARC, respectively. The authors acknowledge the support of Dr. Musarat Ishaq for the cell viability studies.

Appendix A. Supporting information

Supplementary data associated with this article can be found in the online version at http://dx.doi.org/10.1016/j.bios.2016.04.072.

References

Armbruster, D.A., Pry, T., 2008. Clin. Biochem. Rev. 29, S49–S52.
Biswal, M., Banerjee, A., Deo, M., Ogale, S., 2013. Energy Environ. Sci. 6, 1249–1259.
Borghi, F.F., Rider, A.E., Kumar, S., Han, Z.J., Haylock, D., Ostrikov, K., 2013. J. Nanomater. 2013, 1–15.
Cuesta, A., Dhamelincourt, P., Laureyns, J., Martinez-Alonso, A., Tascon, J.M.D., 1998. J. Mater. Chem. 8, 2875–2879.
Gao, L., Ren, W., Xu, H., Jin, L., Wang, Z., Ma, T., Ma, L.-P., Zhang, Z., Fu, Q., Peng, L.-M., Bao, X., Cheng, H.-M., 2012. Nat. Commun. 3, 1–7.
Gong, C., Qu, S., Liu, B., Pan, S., Jiao, Y., Nie, Y., Su, F., Liu, Q., Song, E., 2015. Oncogene 34, 84–93.
Gong, C., Qu, S., Lv, X.-B., Liu, B., Tan, W., Nie, Y., Su, F., Liu, Q., Yao, H., Song, E., 2014. Nat. Commun. 5, 1–15.
Guermoune, A., Chari, T., Popescu, F., Sabri, S.S., Guillemette, J., Skulason, H.S., Szkopek, T., Siaj, M., 2011. Carbon 49, 4204–4210.
Hernandez, Y., Nicolosi, V., Lotya, M., Blighe, F.M., Sun, Z., De, S., McGovern, I.T., Holland, B., Byrne, M., Gun'Ko, Y.K., Boland, J.J., Niraj, P., Duesberg, G., Krishnamurthy, S., Goodhue, R., Hutchison, J., Scardaci, V., Ferrari, A.C., Coleman, J.N., 2008. Nat. Nano 3, 563–568.
Hong, B.J., Compton, O.C., An, Z., Eryazici, I., Nguyen, S.T., 2012. ACS Nano 6, 63–73.
Hsiao, M.-C., Liao, S.-H., Yen, M.-Y., Teng, C.-C., Lee, S.-H., Pu, N.-W., Wang, C.-A., Sung, Y., Ger, M.-D., Ma, C.-C.M., Hsiao, M.-H., 2010. J. Mater. Chem. 20, 8496–8505.
Hu, Y., Wang, K., Zhang, Q., Li, F., Wu, T., Niu, L., 2012. Biomaterials 33, 1097–1106.
Lespade, P., Al-Jishi, R., Dresselhaus, M.S., 1982. Carbon 20, 427–431.
Li, D., Muller, M.B., Gilje, S., Kaner, R.B., Wallace, G.G., 2008. Nat. Nano 3, 101–105.
Niyogi, S., Bekyarova, E., Itkis, M.E., Zhang, H., Shepperd, K., Hicks, J., Sprinkle, M., Berger, C., Lau, C.N., de Heer, W.A., Conrad, E.H., Haddon, R.C., 2011. Nano Lett. 10, 4061–4066.
Novoselov, K.S., Falko, V.I., Colombo, L., Gellert, P.R., Schwab, M.G., Kim, K., 2012. Nature 490, 192–200.
Ostrikov, K., Neyts, E.C., Meyyappan, M., 2013. Adv. Phys. 62, 113–224.
Peng, C., Hu, W., Zhou, Y., Fan, C., Huang, Q., 2010. Small 6, 1686–1692.
Ruan, G., Sun, Z., Peng, Z., Tour, J.M., 2011. ACS Nano 5, 7601–7607.
Seo, D.H., Han, Z.J., Kumar, S., Ostrikov, K., 2013. Adv. Energy Mater. 3, 1316–1323.
Seo, D.H., Pineda, S., Yick, S., Bell, J., Han, Z.J., Ostrikov, K., 2015. Green Chem. 17, 2164–2171.
Shrivastava, A., Gupta, V., 2011. Chron. Young Sci. 2, 21–25.
Suk, J.W., Kitt, A., Magnuson, C.W., Hao, Y., Ahmed, S., An, J., Swan, A.K., Goldberg, B. B., Ruoff, R.S., 2011. ACS Nano 5, 6916–6924.
Sun, Z., Yan, Z., Yao, J., Beitler, E., Zhu, Y., Tour, J.M., 2010. Nature 468, 549–552.
Suni, I.I., 2008. Trends Anal. Chem. 27, 604–611.
Turner, A.P.F., 2013. Chem. Soc. Rev. 42, 3184–3196.
van der Laan, T., Kumar, S., Ostrikov, K., 2015. Nanoscale 7, 20564–20570.
Wang, K., Fishman, H.A., Dai, H., Harris, J.S., 2006. Nano Lett. 6, 2043–2048.
Wang, Y., Alsmeyer, D.C., McCreery, R.L., 1990. Chem. Mater. 2, 557.

Yang, X., Niu, G., Cao, X., Wen, Y., Xiang, R., Duan, H., Chen, Y., 2012. J. Mater. Chem. 22, 6649–6654.
Yick, S., Han, Z.J., Ostrikov, K., 2013. Chem. Commun. 49, 2861–2863.
Zhang, J., Li, A., Yu, X., Guo, W., Zhao, Z., Qiu, J., Mou, X., Claverie, J.P., Liu, H., 2015. Adv. Mater. Interfaces 2, 1–6.
Zhang, Z., Luo, L., Chen, G., Ding, Y., Deng, D., Fan, C., 2014. Biosens. Bioelectron. 60, 161–166.
Zurutuza, A., Marinelli, C., 2014. Nat. Nano 9, 730–734.

Please cite this article as: Pineda, S., et al., Biosensors and Bioelectronics (2016), http://dx.doi.org/10.1016/j.bios.2016.04.072